

Synthesis, phase transition, and magnetic property of iron oxide materials: effect of sodium hydroxide concentrations

Xiaohui Guo · Shengliang Zhong · Ji Zhang ·
Wany Wang · JianJiang Mao · Gang Xie

Received: 24 February 2010/Accepted: 21 June 2010/Published online: 1 July 2010
© Springer Science+Business Media, LLC 2010

Abstract In this paper, a class of novel iron oxide particles has been fabricated through surfactant-directed structure approach in hydrothermal reaction. The obtained iron oxide nanostructures with distinct morphologies, such as rhombohedra, octahedral, plate-like, as well as dendritic, can be obtained by gradually increasing the concentrations of NaOH. The as-prepared iron oxide particles were characterized utilizing scanning electronic microscopy (SEM), X-ray diffraction (XRD), and transmission electron microscopy (TEM). Results reveal that the as-made particles, such as rhombohedra and octahedral, can be indexed as pure rhombohedral phase of hematite and show better single crystalline feature. In contrast, when NaOH concentrations are 1.05 and 6 M, respectively, we accordingly can obtain novel flake-like and dendritic superstructure that possess a mean arm length of $\sim 1.5 \mu\text{m}$; both the as-made two samples can be easily indexed as a mixture of hematite and maghemite based on their XRD and TEM results. Additionally, it was found that the obtained iron oxide

samples at different NaOH concentrations show obviously morphologies-dependent feature. Namely, the as-made samples can undergo transition from typical ferromagnetic to ferrimagnetic behavior when the NaOH concentrations are gradually increased. In general, the presented synthesis approach could be extended to prepare other metal oxides with specific morphology and structure.

Introduction

Metallic oxides nanocrystals (NCs) with adjustable shapes and sizes have attracted a great deal of attention due to their theoretical as well as technological applications in the past decades. Specially, it has been widely accepted that NCs with uniform shape and narrow size distribution are favorable building blocks for the preparation of nanodevices, and they are essential to the advance of nanoscience and nanotechnology [1–7].

In particular, the generation of nanostructure magnetic materials with controllable morphologies and phase is of very significant importance due to their potential applications, which is ranged from ferrofluids, advanced magnetic materials, catalysts, colored pigments, and high-density magnetic recording media to medical diagnostic equipment due to its unique electric and magnetic properties [8–15]. Among magnetic iron oxide NCs, hematite ($\alpha\text{-Fe}_2\text{O}_3$), an n-type semiconductor ($E_g = 2.1 \text{ eV}$), is the most thermodynamically stable phase of iron oxide. It has also showed extensive applications in pigments [16], catalysts [17], gas sensors [18], water treatments [19], and as photoanodes for photo-assisted electrolysis [20] because of its non-toxicity, low processing cost, and highly corrosion-resistant feature. In previous reports, various $\alpha\text{-Fe}_2\text{O}_3$ nanostructures, such as dots [21], rods [22], wires [17], arrays [23], tubes [24],

Electronic supplementary material The online version of this article (doi:[10.1007/s10853-010-4733-8](https://doi.org/10.1007/s10853-010-4733-8)) contains supplementary material, which is available to authorized users.

X. Guo (✉) · J. Zhang · W. Wang · G. Xie
Key Lab of Synthetic and Natural Functional Molecule
Chemistry of Ministry of Education, The College of Chemical &
Materials Science, Northwest University of China,
Xi'an 710069, People's Republic of China
e-mail: guoxh2009@nwu.edu.cn

S. Zhong
The College of Chemistry & Chemical, Jiangxi Normal
University, Nanchang City 330022, China

J. Mao
Department of Chemistry, Fudan University, Shanghai 200433,
People's Republic of China

belts [25], cubes [26], mesopores [27], complex superstructures (e.g. dendrites, propellers, and flowers) [28, 29], as well as their derivative hybrids have already been fabricated via utilizing different synthesis approaches.

At the same time, considerable efforts have been made to the development of nanoscale structures of iron oxide, using a variety of techniques such as chemical precipitation, sol–gel techniques, thermal decomposition of organometallic and coordination compounds, forced hydrolysis, microwave plasma synthesis, reverse micelles, and solid-state reaction [18, 21, 24, 30–35]. Mitra et al. [36] reported that nanospindle, rhombohedron and nanocube structured $\alpha\text{-Fe}_2\text{O}_3$ can be synthesized by the solvothermal method. Hahn et al. [37] synthesized hematite functional films through a solution method. Jia et al. [38] utilized facile one-pot hydrothermal method to synthesize maghemite ($\gamma\text{-Fe}_2\text{O}_3$) nanotubular materials. In addition, literature reported that $\alpha\text{-Fe}_2\text{O}_3$ nanobelts and nanowires materials were fabricated using a gas–solid reaction process [39]. More interestingly, using alumina membrane as the template, some researchers synthesized $\alpha\text{-Fe}_2\text{O}_3$ nanotubes in its ordered and vertical one-dimensional channel structures as the synthetic templates [40]. However, most of the aforementioned approaches tend to involve the use of organometallic precursors, and organic solvents in either potentially hazardous or rather complicated protocol. And also, they usually require complicated operations and sometimes expensive/toxic reagents. This is not favorable to the applications of iron oxide material.

Interestingly, the study on the maghemite to hematite phase transition in the nanoscale regime has been attracted much attention due to the technological applications of maghemite [41]. The phase transition from maghemite to hematite has also been investigated using differential thermal analysis methods [42]. Recently, Raj and co-workers [43] used a simple solution method for producing magnetic nanoparticles with enhanced maghemite to hematite phase transition temperature by controlling the properties of the solvent media. Nevertheless, to the best of our knowledge, there remains a challenge to facile tailoring the morphosynthesis and crystal phase transition from hematite to maghemite of the iron oxide materials that use a mild solution-based approach up-to-date.

In this study, we facile fabricate nearly uniform iron oxide samples with controllable morphologies and crystal phase by simply mediating the sodium hydroxide concentration in the presence of surfactants. And also, it was found that the magnetic properties of the as-made iron oxide samples with distinct morphologies show strong shape-dependent feature. Therefore, we believe that the versatile synthesis strategy may be extended to prepare other metal oxides materials, and promote their further

potential in the fields such as, biological, electronic, and catalysis.

Experimental section

All chemicals are of analytical grade. Iron (III) nitrate nonahydrate, barium chloride, sodium hydroxide, PVP, CTAB, and polyamylose were purchased from Shanghai Chemical Reagent Company and used as received without further purification.

Synthesis of iron oxide samples

Iron oxide samples were prepared by surfactant directing-structure approach. Briefly, 4.50 g of iron (III) nitrate nonahydrate, 1.80 g of barium chloride, and desired amount of surfactants including Polyvinylpyrrolidone (PVP, Mn = 40,000 g/mol), or cetyltrimethylammonium bromide (CTAB) and polyamylose were dissolved in 60 mL of deionised water under magnetic stirring. And then, the different desired concentrations of sodium hydroxide that ranged from 0 to 6 M was added to above homogeneous solution followed by strong stirring continuously for 0.5 h under magnetic interaction, and then, forming homogeneous brown-black solution. Afterwards, it was transferred to a Teflon-lined stainless-steel autoclave and sealed to heat at 180 °C. After reaction for 24 h, the autoclave was naturally cooled to room temperature. The obtained red brown products were centrifuged, then rinsed with water and ethanol for three times, respectively, and finally dried in vacuum at 60 °C for 12 h to obtain final iron oxide samples.

Characterizations

Powder X-ray diffraction (XRD) patterns were recorded on a Bruker D4 X-ray diffractometer (Germany) with Ni-filtered Cu KR radiation (40 kV, 40 mA). Scanning electron microscopy (SEM) images were taken with a Philips XL30 electron microscope operating at 20 kV. Field-emission scanning microscopy (FE-SEM) was taken with Hitachi S-4800 operating at 1.5 kV. A thin-gold film was sprayed on the sample before the characterization. Transmission electron microscopy (TEM) images were conducted on a JEOL 2011 microscope (Japan) operated at 200 kV. The sample for TEM measurements was suspended in ethanol and supported onto a holey carbon film on a copper grid. Magnetic measurements were performed on a Quantum Design MPMS-5 superconducting quantum interference device (SQUID) magnetometer.

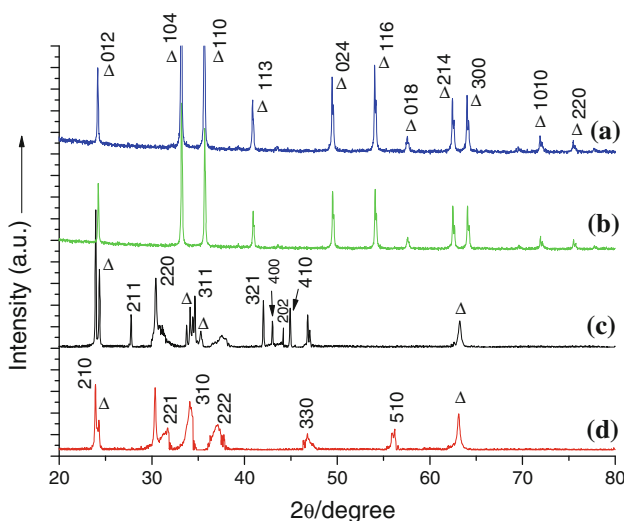


Fig. 1 The wide-angle XRD patterns of the iron oxide samples formed at different sodium hydroxide concentrations (M). (a) 0; (b) 0.35; (c) 1.05; (d) 6.0. Herein, open triangles represent hematite phase

Results and discussion

X-ray diffraction (XRD) patterns of iron oxide samples formed via using PVP as structure-directed template at different sodium hydroxide concentrations (C_{NaOH}) were shown in Fig. 1. Herein, when the concentrations of sodium hydroxide were 0 and 0.35 M, respectively, all the corresponding XRD patterns diffraction peaks can easily be indexed to pure rhombohedral phase of hematite according to standards JCPDS card: 33-0664, results were shown in Fig. 1a, b. In addition, these narrow sharp diffraction peaks indicate that the as-made hematite products are highly crystalline. And no other impurity peaks were detected from Fig. 1a, b. Moreover, when the C_{NaOH} was increased

to 1.05 M, the corresponding XRD pattern of the as-made iron oxide sample can be indexed to a mixture phase of hematite and maghemite, which can be further confirmed by previous study report [20], and was shown in Fig. 1c, wherein, the as-made iron oxide sample shows polycrystalline feature. Moreover, when C_{NaOH} was increased to 6 M, the corresponding XRD pattern behave in a similar trend as in with the case of Fig. 1c, the as-made iron oxide samples can be obviously indexed to mixture of maghemite and trace amount of hematite. Where, the intensity of the main diffraction peaks was obviously higher compared to that of the case in Fig. 1c, and possess smaller amount of hematite compared to that of $C_{\text{NaOH}} \sim 1.05$ M (Fig. 1d). Demonstrating that the crystal phase of the as-made samples can transform from pure hematite to mixture of hematite and maghemite with gradually increasing the sodium hydroxide concentrations in solution.

The morphologies and structure of iron oxide particles prepared using PVP as template in the presence of sodium hydroxide concentrations variation were shown in Fig. 2. When no sodium hydroxide was added, a kind of irregular rhombohedra particle was obtained, the mean size of the as-made sample was about several hundreds of nm, in addition, the surface of rhombohedra particle shows obviously layered feature (Fig. 2a). With C_{NaOH} increasing to 0.09 M, a class of nearly uniform rhombohedra particles can be observed in Fig. 2b, the average size of the as-made particle was around ~ 400 nm, and also the as-made particle possess obvious rough surface feature. Interestingly, while C_{NaOH} was increased to 0.35 M, a kind of novel uniform octahedral-like particle can be obtained (Fig. 2c), the mean size of the as-made particle was about ~ 280 nm, and the surface of the as-made sample was almost smooth. However, when C_{NaOH} was further increased to 1.05 M, a

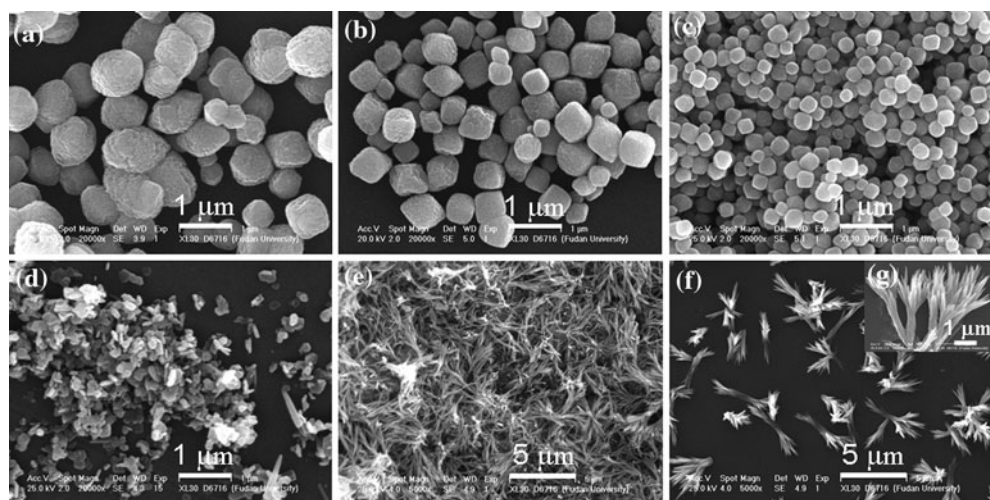


Fig. 2 SEM images of distinct iron oxide particles formed in the presence of sodium hydroxide concentrations variation (M), (a) 0; (b) 0.09; (c) 0.35; (d) 1.05; (e, f, g) 6. Reactions were performed at 180 °C for 24 h, $C_{\text{PVP}} = 2$ g L⁻¹

class of plate-like structure was observed from Fig. 2d, the average thickness was measured to be ~ 80 nm. More particularly, by further increasing C_{NaOH} to 6 M, a high yield of iron oxide sample with unique dendritic structure can be obtained (Fig. 2e, f), the dendritic-like structure was very similar to a multiple-arm plant, the single so-called arm is measured to be ~ 1.5 μm in length (Fig. 2g), which resembles to the pine-tree hematite that was formed using $\text{K}_3[\text{Fe}(\text{CN})_6]$ as iron precursor through hydrothermal reaction [28]. Suggesting the anisotropic growth predominated with varying sodium hydroxide concentrations in solution can indeed exert significant role in mediating the morphosynthesis of the as-made iron oxide samples.

In contrast, if only changing the content of PVP added, while the other conditions were kept constant, we can obtain several distinct morphologies of iron oxide particles (see supporting information Fig. S1). Namely, when $C_{\text{PVP}} = 4 \text{ g L}^{-1}$, a nearly nanocube iron oxide particles with a broader size distribution ranging from several tens of nanometers to micrometers level scope can be observed (Fig. S1a) that maybe resulted from the surfactant encumbrance. With the content of PVP added being decreased, $C_{\text{PVP}} = 1 \text{ g L}^{-1}$, irregular but nearly nanocube hematite particles with coarse surface that formed by aggregation of many small-sized particles, hematites with some defects or grooves on the surfaces can be obtained (Fig. S1b). It was indicated that the specific interaction between PVP and growing crystal planes of primary particles is not strong enough to restrain the intrinsic growth habit [44, 45]. However, when no PVP was added, peach-like iron oxide particles and a few amounts of nearly nanocube particles can be observed in Fig. S1c. Which further confirms the specific interaction of capping agent-PVP with different growing crystal planes indeed play an important role in altering the morphologies of the as-made samples. Note that the selective adsorption of PVP on iron oxide surface plays a crucial role on the crystal growth. Importantly, due to the PVP possess many five-multiple nitrogen heterocycle and longer molecular chain segments, the specific stereo block effect may also result in the morphology-selective preferable growth.

Specially, we also investigate the effect of BaCl_2 on the morphology of the obtained iron oxide samples; result was shown in supporting information Fig. S2. When no BaCl_2 was added into the reaction system, only irregular iron oxide aggregated particles were obtained in the case of $C_{\text{NaOH}} = 0.35 \text{ M}$ (supporting information Fig. S2b), in contrast, a class of unique nearly octahedral-shaped particles can be obtained when 1.80 g of BaCl_2 was added into the same reaction system (supporting information Fig. S2a). Indicating the addition of BaCl_2 can indeed significantly affect the morphogenesis of the as-made iron oxide samples.

In the meanwhile, for comparison, we should further explore the influence of the surfactant templates with distinct functional groups on the morphologies and structures of the as-made samples. Wherein, when using CTAB and polyamylose as dual templates, other reaction conditions were identical to that described in Fig. 2c. We can obtain a kind of nearly spherical particle with many surface defects, and was shown in supporting information Fig. S3, the as-made particle was ranged from 80 to 700 nm in diameter (Fig. S3b). Additionally, the as-made particles can be readily indexed as pure hematite phase and possess single crystalline feature (Fig. S4). If only using CTAB as template-agent, a uniform rhombohedra or cube particles can be formed according to previous literature report [26].

In order to gain detailed microstructure information and speculate the possible growth mechanism of the as-made novel dendritic-like structure, a small amount of dendritic-like iron oxides were dispersed in water and ultrasonically treated in a water bath for several minutes for TEM characterization. Figure 3a shows a typical SEM image of dendritic samples with high yield. After ultrasonic treatment of the dendritic sample for several minutes, a patch of dendritic structure can be obtained (Fig. 3b), indicating that the unique dendritic structure was composed of many irregular rods with a tip end. In addition, the corresponding HRTEM image of the single rod-like tip end was performed (Fig. 3c); its spacing was measured to be $\sim 3.01 \text{ \AA}$, corresponding to 220 crystal planes. It was seen that the rod possess obvious crystal lattice stripe and better polycrystalline feature. Moreover, the dendritic sample can undergo preferable orientated growth along (220) crystal faces (Fig. 3d), it shows a obvious diffraction ring feature from Fig. 3d, which agrees well with the above XRD result described in Fig. 1d. Apart from that, the EDS result performed further confirms the chemical composition of the as-made sample, as shown in Fig. 3e (Table 1).

Possible formation mechanism of iron oxide with distinct morphologies proposed

As described above, The NaOH concentration was found to be a very important synthetic parameter to influence the phase transition between maghemite and hematite. Namely, when the NaOH concentrations ranged from 0 to 6 M, the morphologies and the phases of the as-prepared products are totally different, which can be confirmed from Figs. 1 and 2. And also, it seems that the maghemite phase gradually becomes the predominant phase when the NaOH concentration is further increased, which is slightly inconsistent with that of the previous literature report [46], demonstrating this anisotropic growth predominated at higher alkaline condition. When the sodium hydroxide

Fig. 3 Typical SEM image (**a**); TEM image (**b**); HRTEM image (**c**) was taken from the selected area located in (**b**); (**d**) selected area electron diffraction (SAED) image (*inset*); (**e**) energy dispersion spectrum (EDS) of the dendritic-shaped iron oxide samples formed at $C_{\text{NaOH}} = 6 \text{ M}$

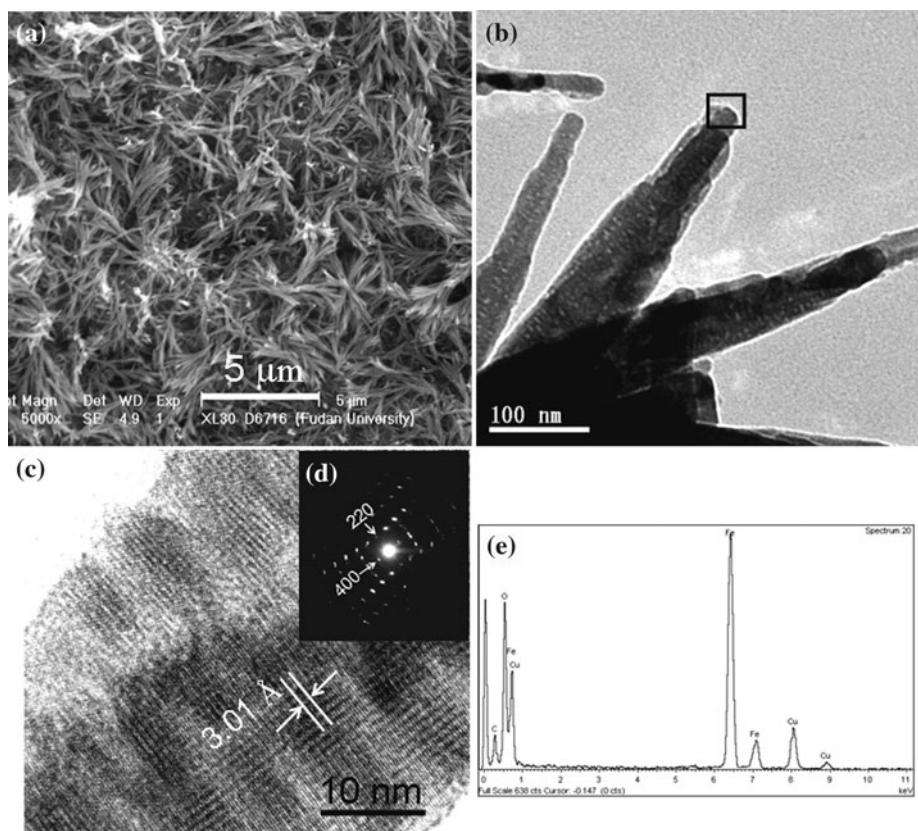


Table 1 Summary of iron oxide samples obtained at different NaOH concentrations (M) in the presence of PVP

Sample number	C_{NaOH}	Phase	Morphologies	Average size
1	0	Hematite	Irregular rhombohedra	~850 nm
2	0.09	Hematite	Regular rhombohedra	~650 nm
3	0.35	Hematite	Octahedral-like	~280 nm
4	1.05	Hematite + maghemite	Plate-like	~80 nm ^a
5	6	Hematite ^c + maghemite	Dendritic	~1.5 μm ^b

^a The average thickness of the as-made plate-like sample

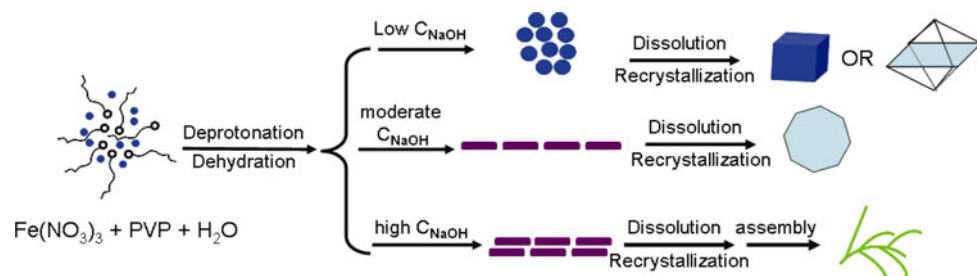
^b The average length of an single arm of the as-made dendritic structure

^c Trace amount of hematite

concentration is lower, only rhombohedra or octahedral particles can be formed through a dissolution and recrystallization process of precursor, then, the as-formed precursor was FeOOH nanocluster, which agrees well with the case of CTAB-mediated the formation of rhombohedra hematite in hydrothermal reaction [26]. With the NaOH concentration gradually increasing, it was assumed that the precursor morphologies change from spherical nanoparticle to rod or sheet, the pH of hydrolyzed Fe(III) solutions increases gradually, which accelerates the rate of the hydrolysis of Fe(III) ions and further favors its overgrowth of the FeOOH precursor in higher alkaline condition, leading to the final formation of the plate or dendritic structures, which can resemble the case of the shuttle-like

barium carbonate formed in higher surfactant concentrations [47]. Moreover, the higher NaOH concentration can suppress the formation of hematite phase due to higher chemical potential that favors anisotropic growth of the precursor, and eventually leading to the formation of dendritic-like superstructure, as highlighted by Peng et al. [48] Herein, we therefore propose a “nucleation–aggregation–dissolution–recrystallization–overgrowth” mechanism that is mainly responsible for the formation of the iron oxide with distinct morphologies and phase. The whole formation process of iron oxide samples formed in the presence of sodium hydroxide concentrations variation was shown in Scheme 1. Of course, the Ostwald ripening process and the structure-directed surfactants can be helpful to the

Scheme 1 The formation process of iron oxide samples formed in the presence of sodium hydroxide concentrations variation



formation of iron oxide samples with different morphologies (Scheme 1).

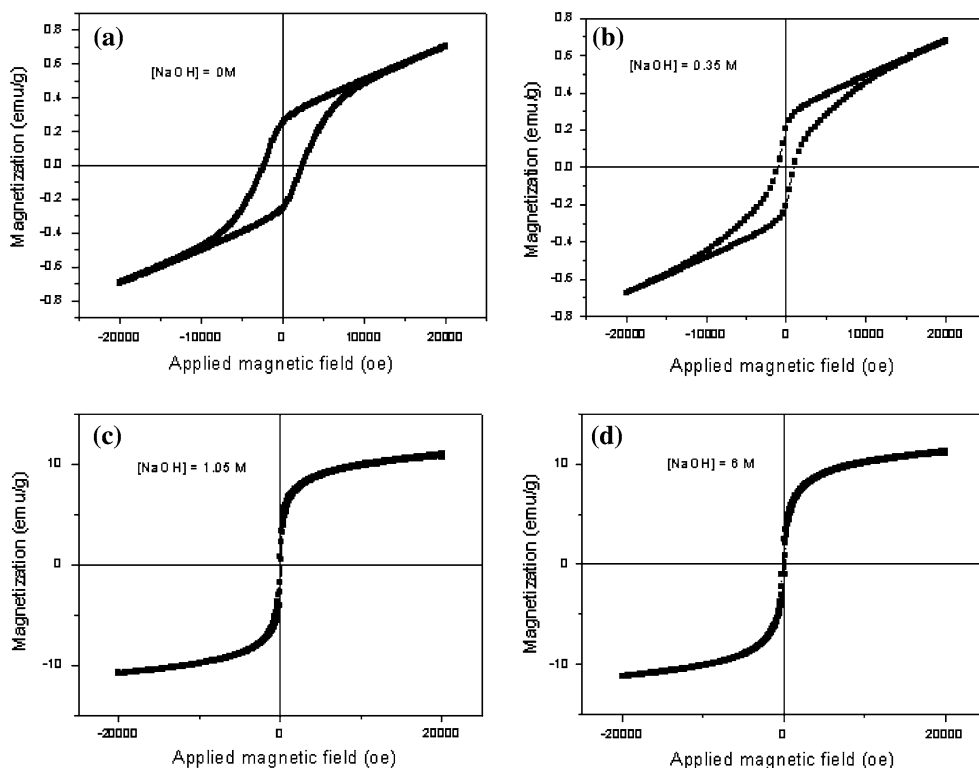
When no NaOH was added, the as-made sample exhibit a typical paramagnetic behavior due to the presence of pure hematite component, the case is almost the same as that in previous report [46, 49], as shown in Fig. 4a, its magnetization is about ~ 0.69 emu/g, its remained coercive force magnitude is measured to be about ~ 2400 Oe with an applied external magnetic field of ~ 20000 Oe (Fig. 4a). Similarly, while C_{NaOH} was increased to 0.35 M, the as-made sample can also behave as a similar paramagnetic feature, as shown in Fig. 4b, its magnetization is measured to be ~ 0.68 emu/g, its remained coercive force magnitude is measured to be about ~ 1000 Oe (Fig. 4b). However, the samples formed at higher NaOH concentrations, namely, when C_{NaOH} are 1.05 and 6 M, respectively, the two as-made samples exhibit a typical ferrimagnetic behavior without a hysteresis loop due to the existence of most of

maghemite [20, 50], results were shown in Fig. 4c, d, their corresponding saturation magnetizations are 10.76 and 11.27 emu/g, respectively, suggesting that the formation of part maghemite phase and thermal energy can overcome the anisotropy energy barrier of a single particle. Notably, it was obviously found that the magnetic behavior of the as-made iron oxide samples are strongly dependent on their morphologies and structures.

Conclusions

In summary, we have successfully prepared a series of iron oxide samples with distinct morphologies and phase behavior in the presence of surfactants and sodium hydroxide concentrations variation at mild reaction solution. Wherein, such as rhombohedra, octahedral, spherical, plate-like, as well as dendritic superstructure can be

Fig. 4 M - H curves of the as-synthesized iron oxide materials obtained in the presence of sodium hydroxide concentration variations, (a) 0 M, (b) 0.35 M, (c) 1.05 M, (d) 6 M



obtained by simply adjusting the concentration of sodium hydroxide in solution. And also, the high yield of dendritic iron oxide product was for the first time reported till now. While the NaOH concentration was gradually increasing, the crystal phase of the as-made samples can undergo transformation from pure hematite to mixture of hematite and maghemite, the corresponding magnetic property of the as-made samples show a obvious change, occurring the transformation from typical ferromagnetic to almost complete ferrimagnetic while increasing the sodium hydroxide concentrations. In general, the presented synthesis route is mild and simple, which may be further extended to the preparation of other metal oxides nanostructures with specific morphologies and function specialty.

Acknowledgements This work was supported by China Postdoctoral Scientific Fund (No. 20070420085), Research startup fund of northwest University (No. PR09047), Education committee of Shanxi Province (Grant No. 09JS089), and the National base Science cultivate Foundation of China (No. J0830417).

References

1. Sun SH, Murray CB, Weller D, Folks A (2000) *Science* 287:1989
2. Sun SH, Zeng H, Robinson DB (2004) *J Am Chem Soc* 126:273
3. Kuroda S, Nishizawa N, Takita K, Mitome M, Bando Y, Osuch K, Dietl T (2007) *Nat Mater* 6:440
4. Mackenzie JD, Bescher EP (2007) *Acc Chem Res* 40:810
5. Sakatani Y, Boissiere C, Grosso D, Nicole L, Soler-IIIa AA, Sanchez C (2008) *Chem Mater* 20:1049
6. Sun Y, Xia Y (2002) *Science* 298:2176
7. Sun YG, Mayers BT, Xia Y (2002) *Nano Lett* 2:481
8. Gaidide Y, Kravchuk VP, Sheka D (2010) *Int J Quantum Chem* 110:83
9. Hyeon T (2003) *Chem Commun* 927
10. Liu XH, Guo Y, Wang YG (2010) *J Mater Sci* 45:906. doi: [10.1007/s10853-009-4019-1](https://doi.org/10.1007/s10853-009-4019-1)
11. Kim J, Lee JE, Lee SH, Yu JH, Lee JH, Park TG, Hyeon T (2008) *Adv Mater* 20:478
12. Veronica SM, Miguel CD (2007) *Adv Mater* 19:4131
13. Zhao S, Wu HY, Song L (2009) *J Mater Sci* 44:926. doi: [10.1007/s10853-008-3192-y](https://doi.org/10.1007/s10853-008-3192-y)
14. Gaihre B, Khil MS, Ko JA (2008) *J Mater Sci* 43:6881. doi: [10.1007/s10853-008-3003-5](https://doi.org/10.1007/s10853-008-3003-5)
15. Yang Y, Jiang JS (2008) *J Mater Sci* 43:4340. doi: [10.1007/s10853-008-2609-y](https://doi.org/10.1007/s10853-008-2609-y)
16. Lin CK, Li Y, Yu M, Yang P, Lim J (2007) *Adv Funct Mater* 17:1459
17. Hu XL, Yu JC, Gong JM, Li Q, Li GS (2007) *Adv Mater* 19:2324
18. Xiong Y, Li Z, Li X, Hu B, Xie Y (2004) *Inorg Chem* 43:6540
19. Cesar I, Jose AK, Martinez G, Gratzel M (2006) *J Am Chem Soc* 128:4582
20. Zhong LS, Hu JS, Liang HP, Cao AM, Song WG, Wan LJ (2006) *Adv Mater* 18:2426
21. Cao HQ, Wang GZ, Zhang L, Liang L, Zhang SC, Zhang XR (2006) *Chem Phys Chem* 7:1897
22. Woo K, Lee HJ, Ahn JP, Park YS (2003) *Adv Mater* 15:1761
23. Vayssières L, Sathe C, Butorin SM, Shuh DK, Nordgren J, Guo JK (2005) *Adv Mater* 17:2320
24. Zhou HJ, Woo SS (2008) *ACS Nano* 2:944
25. Zhao YM, Li YH, Ma RZ, Roe MJ, McCarten DG, Zhu YQ (2006) *Small* 2:422
26. Pu ZF, Cao MR, Yang J, Huang KL (2006) *Nanotechnology* 17:799
27. Anda M, Shamshuddin J, Fauziah IC, Omar SRS (2008) *Soil Sci* 173:560
28. Cao MH, Liu TF, Gao S, Sun GB, Wu XL, Hu CW, Wang ZL (2005) *Angew Chem Int Ed* 44:4197
29. Liu XH, Guo JJ, Cheng YC, Li Y, Xu GJ, Cui P (2008) *J Cryst Growth* 311:147
30. Matijetivic E (1981) *Acc Chem Res* 14:22
31. Elkins KE, Vedantam TS, Liu JP, Zeng H, Sun SH, Ding Y, Wang ZL (2003) *Nano Lett* 3:1647
32. Song HM, Ko JM, Park JH (2009) *Chem Lett* 38:612
33. Park TJ, Wong SS (2006) *Chem Mater* 18:5289
34. Song Q, Zhang ZJ (2004) *J Am Chem Soc* 126:6164
35. Lattuada M, Hatton TA (2007) *Langmuir* 23:2158
36. Mitra S, Das S, Mandal K, Chaudhuri S (2007) *Nanotechnology* 18:275608
37. Hahn NT, Ye HC, Flaherty DW, Bard AJ, Mullins CB (2010) *ACS Nano* 4:1977
38. Jia CJ, Sun LD, Yan ZG, Pang YC, You LP, Yan CH (2007) *J Phys Chem C* 111:13022
39. Wen XG, Wang SH, Ding Y, Wang ZL, Yang SH (2005) *J Phys Chem B* 109:215
40. Lahav M, Schayek T, Vaskeich A, Rubinstein I (2003) *Angew Chem Int Ed* 42:5576
41. Clark SM, Prilliman SG, Erdonmez CK, Alivisatos AP (2005) *Nanotechnology* 16:2813
42. Kulkarni NV, Karmakar S, Banerjee I, Sahasrabudhe SN, Das AK, Bhoraskar SV (2009) *Mater Res Bull* 44:581
43. Gnanaprakash G, Ayyappan S, Jayakumar T, Philip J, Raj B (2006) *Nanotechnology* 17:5851
44. Hu XL, Yu JC (2008) *Adv Funct Mater* 18:880
45. Guo XH, Deng YH, Gu D, Che RC, Zhao DY (2009) *J Mater Chem* 19:6706
46. Liang X, Wang X, Zhuang J, Chen YT, Wang DS, Li YD (2006) *Adv Funct Mater* 16:1805
47. Guo XH, Xu AW, Yu SH (2008) *Cryst Growth Des* 8:1233
48. Peng ZA, Peng XG (2001) *J Am Chem Soc* 123:1389
49. Bhagwat S, Singh H, Athawale A (2007) *J Nanosci Nanotechnol* 7:4294
50. Palotas K, Andriotis AN, Lappas A (2010) *Phys Rev B* 81:075403